RESEARCH Open Access

Flood and landslide susceptibility assessment and multi hazard interaction mapping using machine learning and GIS for sustainable settlement planning in Nepal

Narayan Thapa[1], Kabir Uddin[1], Rajesh Bahadur Thapa[1] and Erica Udas[1*]

*Correspondence:
Erica Udas
erica.udas@icimod.org
[1]International Centre for Integrated Mountain Development, Kathmandu, Nepal

Abstract
Nepal lies within an active seismic zone and is influenced by most dynamic climatic systems in the world. It faces compounding floods and landslide threats. Impacts are worst where multi-hazard interactions create spatially linked corridors. Despite frequent co-occurrence, national-scale assessments remain limited. This study presents machine learning and GIS-based approach to map nationwide susceptibility to floods, landslides, and identify their potential interaction zones, and delineate critical multi-hazard flow zones through spatial adjacency analysis. Using Google Earth Engine, the Random Forest model integrates topographic, climatic, environmental, and hydrological datasets to overcome subjective expert-driven methods. The model achieved strong predictive accuracy (AUC: 0.84 for floods, 0.85 for landslides). The results showed 19% of Nepal's lowlands are medium to very highly susceptible to inundation, threatening approximately 900,000 people and over 3.4 million buildings; whilst in the hilly terrains, 40% is susceptible to slope-failure endangering 200,000 people and about 0.6 million buildings. K-means clustering followed by spatial adjacency analysis identified four spatial zonation: 81% of national area as low-hazard zone, 9% as flood-only zone, 5% as landslide-only zone, and 5% as interaction zones. Critical multi-hazard flow zone covering 7,588 km^2 represents spatially connected corridors linking interaction zones to downstream flood-prone populated areas, affecting 88 km^2 built-up land and 1,722 km^2 cropland. These zones represent susceptibility-based spatial connectivity rather than physically simulated cascading processes. These findings support recommendations for risk-informed land-use planning, resilient infrastructure development and climate adaptation aligned to sustainable development and investment risk screening.

Keywords Remote sensing, Multi-hazard, Risk zoning, Machine learning, Mountain development, Spatial planning

1 Introduction

The Hindu Kush Himalaya (HKH) is one of the most disaster-prone regions in the world, where active seismic zones, extreme topographic gradients, seasonal monsoon-driven precipitation, and fragile geological formations intersect, creating a highly biodiverse region with a dynamic risk landscape [1]. This risk landscape is fundamentally influenced by complex socio-ecological systems that require urgent action to sustain the mountain environment. Nepal frequently experiences compound natural hazards, particularly from floods and landslides, that often interact and produce sequential events from upstream to downstream [2]. These events are largely attributed to young mountainous terrain in seismically active zones, rapid unplanned urbanization, and climate change, all of which create conditions for natural disasters and hazards threatening people's lives, property and infrastructures [3–6]. Such compounding effects may occur simultaneously or evolve over time through interconnected processes. For instance, intense monsoon rainfall can concurrently trigger flooding and landslides. Moreover, time-dependent causes include forest fires that destabilize slopes, often resulting in debris flows [7], and earthquakes that can directly trigger landslides or landslide dam outburst floods [8]. Likewise, permafrost thawing eliminates subsurface ice cohesion, directly triggering catastrophic mountain slope failures [9]. The Melamchi flood in 2021 represents such a catastrophic source-to-sink disaster in Nepal, caused by sequential events involving heavy upstream precipitation, landslides and debris flow [10–12].

Disasters are thus no longer defined by natural extremes, but by complex interactions among multiple hazards, social vulnerability, and systemic governance gaps [2]. Because floods and landslides can occur in the same region, this study seeks to identify their interactions as the resulting multi-hazard flow zones currently remain poorly characterized. Given that decision makers face challenges in responding to single hazard, responding to multi-hazard events requires a systemic understanding of interactions and interrelationships that trigger sequential hazard events. However, the concept of compounding and interacting sequential or cascading effects is relatively new in natural risk governance having limited methodologies and field applications; yet it is critical for understanding cumulative damage, where multiple hazards affect the same element increasing the risks to people's lives, infrastructure, and economy systems [13–16]. In simple terms, such events can be understood as a snowball process, in which an initial trigger evolves into a series of adverse outcomes, and each branch of the event tree represents a cause-and-effect chain that amplifies vulnerability [13]. Nevertheless, simulating such physical cascading dynamics is beyond the scope of this study, instead, the paper provides a screening-level spatial adjacency framework that identifies places where landslide susceptible upstream areas are geographically connected to flood susceptible downstream zones.

Although Nepal has advanced in developing national and local disaster risk management strategies [17], it still lacks a national level understanding of multi-hazard spatial interaction where floods and landslides intersect to form critical multi-hazard flow zones. In an evolving multi-hazard risk landscape, such evidence is crucial for long-term planning of human settlements, investments to critical infrastructure projects, livelihood opportunities, and emergency preparedness. Multi-hazard flow zones are physically linked to sediment mobilized from landslide-prone headwaters that travel through tributary networks into flood-prone valleys [18], transforming localized slope failures into downstream hazards [19]. These sequential events indicate that disaster risk in mountainous terrain is regulated not only by the magnitude of individual hazards but also their spatial connectivity. Furthermore, drivers such as rapid unplanned urbanization disrupt the fragile physical connectivity between hillslope processes and fluvial systems, accelerating the impact.

Despite growing scientific consensus that floods and landslides operate as a physically coupled system, natural hazard governance in Nepal remains structurally siloed. This is clearly demonstrated by the separate jurisdictional roles of the Department of Hydrology and Meteorology (DHM), who manages flood hazards, and the Department of Mines and Geology (DGM), who oversees landslide hazard management. This institutional isolation in the absence of collective action, treats interconnected hazards as spatially and administratively separate phenomena, creating a critical blind spot in disaster risk reduction and risk-informed decision-making. Yet, the geomorphic reality remains that landslide-prone slopes and flood-prone channels often share contiguous boundaries at the slope-toe interface, where debris from the slope failures enter the drainage network and can exacerbate downstream inundation [18]. Thus, understanding these interactions requires moving beyond static hazard overlays toward frameworks that explicitly recognize how upstream slope instability can precondition or amplify downstream flood risk through topographically controlled hazard flow pathways.

Furthermore, mountainous communities are disproportionately exposed to hazards because settlements, roads, and critical infrastructures, such as road networks, hydropower etc. frequently occupy transition zones between steep slopes and active river channels [20–22]. Identifying susceptible zones where landslide-prone upstream areas and flood-prone downstream zones intersect is therefore crucial for ensuring the safety and resilience of local communities, as well as for planning resilient infrastructure development and risk-informed decision-making. This paper addresses the gap through initial screening-level spatial adjacency framework that maps susceptibility-based interaction zones and delineates multi-hazard flow zones in corridors, where upstream landslide-susceptible areas are spatially linked to downstream flood-susceptible settlements, without requiring computationally intensive process-based simulations. This work also closely aligns with global frameworks including the Sendai Framework for Disaster Risk Reduction and the Sustainable Development Goals (SDG 9, SDG 11, SDG 13), emphasizing an evidence base, data-driven long-term planning for sustainable cities and human settlements, resilient infrastructure investments, and climate actions for risk mitigation, early warning systems and emergency preparedness [23–25].

Past studies in Nepal have primarily used Geographic Information System (GIS) based multi-criteria analysis (MCA) to assess individual hazards, relying on expert-defined weights for variables such as slope, land cover, elevation, and other parameters [26, 27]. Because this method is inherently subjective and struggles to capture non-linear relationships among hazard variables [28], it was widely used for susceptibility mapping. With advancements in remote sensing and machine learning techniques, contemporary methodologies now address both linear and non-linear relationships among predictor parameters [29]. Recent studies have applied machine learning models to better understand the relationship between rainfall extremes and landslide susceptibility, thereby identifying reinforcement priorities [30]. Other studies investigated process-based multi-hazard dynamics at basin scales by examining landslide dam formation, breach dynamics, and downstream flood propagation [31, 32]. Likewise, multi-hazard frameworks have been developed to support evacuation and shelter allocation by considering the landslides and floods in mountainous areas [33].

In this context, the current paper presents a national-level assessment for Nepal, combining remote sensing and machine-learning-based risk susceptibility mapping to delineate multi-hazard flow zones and assess their integrated impacts on human settlements. It uses Random Forest (RF) model, which provides a data-driven variable-weighting framework to overcome human bias by automatically ranking variable importance [34, 35]. Rather than simulating physical process dynamics, the RF model incorporates topographical, hydrological, land-cover and vegetation characteristics as a key driver [27, 36, 37] and applies unsupervised machine learning to identify the interaction clusters for both floods and landslides. It further generates national-scale susceptibility maps for floods and landslides separately and identifies multi-hazard flow zones in which landslide-prone areas are spatially linked to downstream flood-prone areas.

The objectives of this study are threefold-

- To map national-scale flood and landslide susceptibility using RF machine-learning models and delineate multi-hazard interaction zones and critical multi-hazard flow zones by integrating susceptibility outputs with unsupervised machine learning and GIS-based spatial adjacency analysis.
- To develop a national-scale, screening-level framework for flood-landslide interaction to support evidence-based, risk-informed decision-making for sustainable settlements and infrastructure planning in Nepal.
- To estimate the potential downstream exposure to multi-hazard flow zones and derive spatially explicit policy recommendations.

2 Study area

Nepal, with its diverse topography, complex geography, and highly varying climate, provides an ideal study area for multi-hazard risk susceptibility mapping Fig. 1. Globally, the country is ranked the 4th most climate-vulnerable nation, and it is among the top 20 countries that face multiple hazards, both natural and human-induced [38]. Studies report that an average of two people died daily, and that more than 300 families were affected by disasters each year over the past 50 years [39]. This semicentennial analysis reflects that floods and landslides are major risks reporting an average of 113 deaths per year from landslides only [40] whereas floods cause 9.33% of total disaster-related deaths and affect 61.60% of families annually [39].

3 Data and methodology

3.1 Data used

In this study, freely open-access datasets were used to develop the model for flood and landslide susceptibility mapping in Nepal. Unsupervised machine learning and spatial adjacency analysis were applied to susceptibility datasets to identify the interaction and multi-hazard flow zones. Historical flood and landslide inventories further informed past hazard occurrences for model development.

The topographical datasets used include Digital Elevation Model (DEM), slope, aspect, Terrain Ruggedness Index (TRI), Topographic Wetness Index (TWI), Height Above Nearest Drainage (HAND), and landform categories to capture terrain characteristics

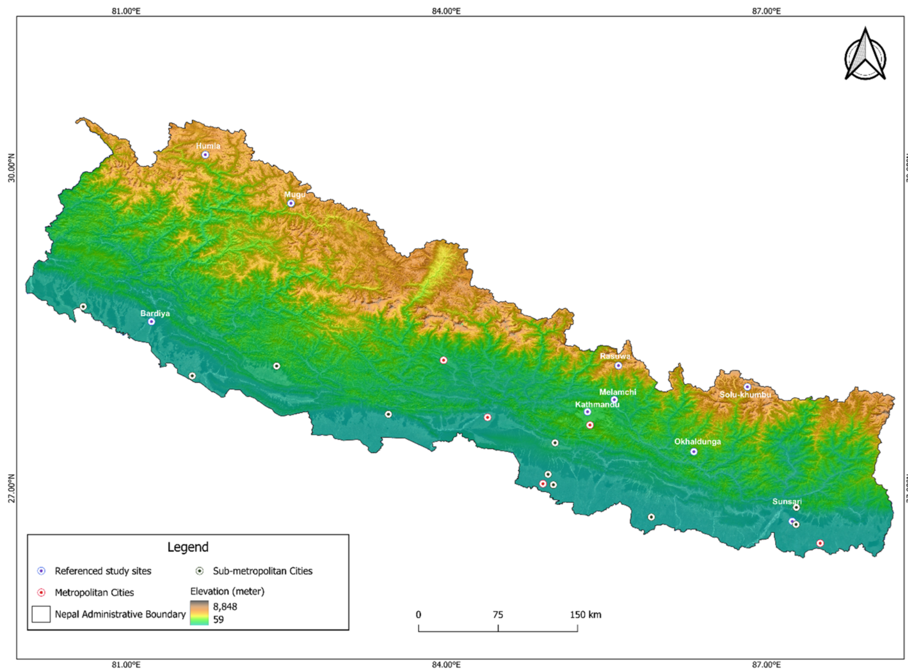

Fig. 1 Study area map showing Nepal's topographic profile derived from digital elevation model data showing metropolitan and sub-metropolitan cities and referenced study sites. (Source of Administrative boundary: Department of Survey, Nepal)

for water flow and slope stability. Land cover data and Normalized Difference Vegetation Index (NDVI) provides information on vegetation and soil exposure. Hydrological datasets (distance from rivers, soil properties, hydraulic conductivity) describe water movement and infiltration. Distance from the roads provides information about anthropogenic flood and landslide drivers. Climate data such as precipitation represents rainfall-driven potential susceptibility. OpenStreetMap (OSM) building and population datasets are used to identify exposure. The dataset details are described in Table 1. Similar parameters have been widely used in past studies for flood and landslide risk susceptibility modelling [41, 42].

3.2 Methodology

The methodology was divided into three primary stages as shown in Fig. 2. In the first stage, flood susceptibility maps were generated using a Random Forest probability model integrated with 11 flood-related conditioning parameters. Similarly, landslide susceptibility was modeled using 12 independent variables.

In the second stage, both models were validated against ground-truth samples and existing inventories, after which parallel analytical tracks were pursued. Track A (single-hazard exposure): susceptibility maps were independently overlaid with building footprints and population data to quantify direct exposure. Track B (Multi-hazard interaction zone): The two-susceptibility data were used as input parameters using unsupervised k-means clustering (k = 3) to categorize the study area into three initial hazard zone classes: low-hazard, flood zone and landslide zone. The interaction zone (fourth class) was subsequently derived through GIS-based spatial adjacency analysis, between flood zone and landslide zone.

Table 1 Data sources for flood and landslide modelling. (see detail maps in Supplementary, S1-S7)

Datasets	Time	Data sources	Resolution	Type	Remarks
Nepal administrative boundary data		Department of Survey Nepal	NA	Administrative	Digitization and vector data processing within a Geographic Information System (GIS)
Flood data	2019 to 2023	[43, 44]	10 m	Hazards inventory	This dataset is based on flood inundation mapping that utilizes Copernicus data and thresholding techniques.
Landslide	1960 to 2017	[45–47]	NA	Hazards inventory	Digitization of high-resolution satellite imagery from Google Earth.
Copernicus Digital Elevation Model	2021	https://dataspace.copernicus.eu/	30 m	Topographical	It is developed from radar collected by the TanDEM-X satellite mission.
HAND	2016	https://www.earthdata.nasa.gov/	30 m	Topographical	The terrain analysis algorithm measures the vertical distance above the nearest water feature.
Landform	2006 to 2011	[48]	30 m	Topographical	It is derived from the Digital Elevation Model with the help of a multi-scale Topographic Position Index and Continuous Heat-insolation Load Index.
OpenStreetMap data (Road, building, River network)	2022	OpenStreetMap	NA	Exposure and anthropogenic	It is created by digitization of high-resolution imageries by global volunteers using a participatory approach.
Precipitation	2018 to 2023	[49]	Resampled 30 m	Climate dataset	It is developed by combining satellite infrared imagery with rain gauge dataset.
Silt and sand	2020	[50]	30 m	Hydrological datasets	The field survey was conducted and re-sample to develop the final product.
Land cover	2021	[51]	30 m		The Landsat dataset was used with an RF classifier to develop the final product.
Hydraulic conductivity	2015	[52]	30 m	Hydrological datasets	Estimated using predictive models, such as Ped transfer function based on soil properties.
Slope	2021	Derived from DEM	30 m	Topographical	It measures the maximum rate of change of elevation using 3*3 moving window on the DEM.
Aspect	2021	Derived from DEM	30 m	Topographical	It is determined from a DEM by identifying the downslope direction of each of the steepest slopes for each cell, measured in degree clockwise from north.
Flow accumulation	2021	Derived from DEM	30 m	Hydrological datasets	It represents the number of upslope cells contributing flow to a given down cell and calculation based on a pre-computed flow direction raster.
Flow direction	2021	Derived from DEM	30 m	Hydrological datasets	Compute from a DEM by identifying the path of steepest descent from each cell to one of its neighbors using D8 flow direction methods.

Table 1 (continued)

Datasets	Time	Data sources	Resolution	Type	Remarks
Terrian Wetness index	2021	Derived from DEM	30 m	Topographical	It is derived from DEM and calculates the natural logarithm of the ratio of the upslope contributing area to the tangent of the local slope.
Terrian Roughness index	2021	Derived from DEM	30 m	Topographical	It calculates the standard deviation of elevation within a 3*3 moving window.
Normalized Difference Vegetation Index using Landsat	2021	Derived from DEM	30 m	Vegetation	It is calculated using the Near infrared and red band
Population	2020	[53]	100 m	Exposure	Global high-resolution population distribution data estimated using random forest model with covariates such as building footprints, landcover and night-time light
100 year return period flood	2017	https://maps.meteor-project.org/map/flood-npl/	30 m	Hazard inventories	The data presented here show the modelled water depth for flood events of different return periods.

NA- Not Applicable as vector data is used

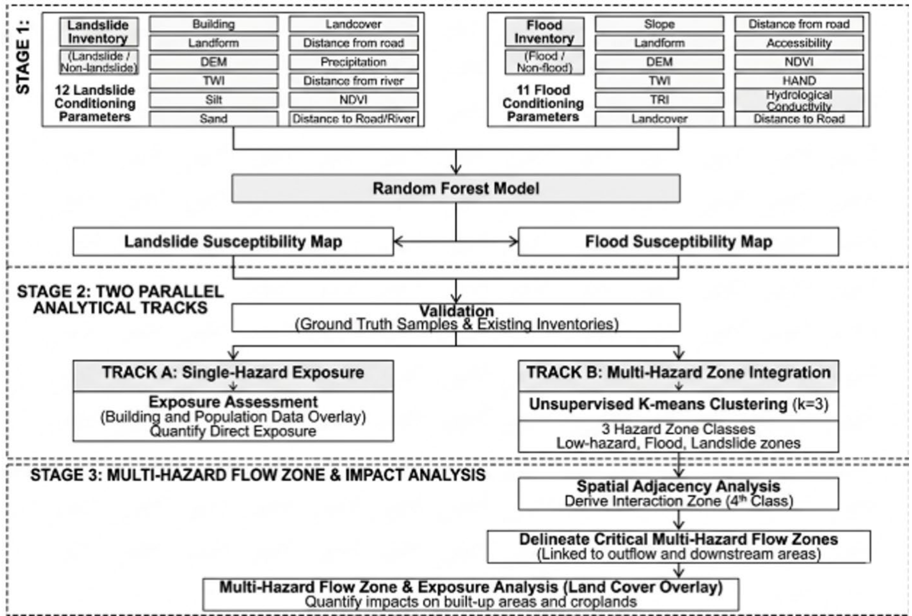

Fig. 2 Methodological flow chart for flood and landslide susceptibility mapping, multi-hazard interaction zone identification, and exposure analysis. The workflow integrates random forest classification (probability output) with k-means clustering (k = 3) and spatial adjacency analysis to delineate interaction zone and multi-hazard flow zones

Finally, a critical multi-hazard flow zone and its impact analyses were conducted. The critical multi-hazard flow zones were delineated by linking interaction zones to downstream flood prone area through sequential spatial adjacency analysis. These flow zones were overlaid with land cover data to quantify impacts on various land cover classes such as, built-up areas and croplands.

3.3 Sampling techniques

After compiling all the required data, stratified random sampling was performed to ensure a more accurate representation of all pixels by dividing them into distinct subgroups using Eq. (1), thereby reducing overfitting and spatial autocorrelation [54]. This sampling strategy was designed to provide at a 99.9% confidence level [55].

$$\mathrm{s} = z^2 * \frac{p(1-p)}{m^2} \tag{1}$$

Here, s is the sample size, z is the z-score corresponding to desired confidence level, and the p is the proportion of pixels in the partition to be used and m is the margin of error.

The adjusted sample size formula is used when the population size is known

$$\text{s-adj} = \frac{s * N}{(s + N - 1)} \tag{2}$$

Here s is the sample size calculated from N, the pixels size and s-adj is adjusted sample size.

The image pixels, covering the whole study area at a resolution of 30 m, represent a total of approximately 163 million pixels. Using Eqs. (1) and (2), the minimum number of samples required was 1,082. However, because 70% of the data was reserved for model training (i.e. 1,120), the total sample size was increased to 1,600 points to ensure the training subsets ($n = 1,120$) exceeded this minimum statistical requirement. Of this total, 70% were used for training, 10% for testing, and 20% for validation.

The flood and landslide inventories were then transformed into point datasets to set up RF probability models. In the case of stratified random sampling, we created a grid with a resolution of 400 m * 400 m, which ensured that samples were distributed across the study area with minimum separation of 400 m. This was applied to minimize errors from spatial autocorrelation effects.

3.4 Random forest model

The study used a RF probability model for flood and landslide susceptibility mapping using the cloud-based Google Earth Engine (GEE) platform. A limited sample size was used for hyperparameter tuning for the number of trees, ranging from 400 to 600, which indicated that the optimal number of trees for best model accuracy was 600. The model deals with binary data, which is flooded versus non-flooded points, and landslide versus non-landslide points then a bootstrapping technique is implemented to construct an ensemble of independent decision trees. Each tree in the forest is trained on a random subset of the 1,120 stratified samples and at every node, a random subset of conditioning factors is evaluated to determine the optimal split.

The model produces continuous outputs ranging from 0 to 1, representing susceptibility scores as shown in Eq. (3).

Mathematically, it is expressed as:

$$f\left(x\right)=\left(\frac{1}{B}\right)\sum\nolimits_{b=1}^{B}fb\left(x\right) \tag{3}$$

Here, $\mathrm{f}\left(x\right)$ is the estimated probability of susceptibility.

B is the number of trees.

$fb\left(x\right)$ is the prediction of the b$^{\mathrm{th}}$ individual tree.

We integrated various environmental variables for flood and landslide susceptibility mapping. This ensemble approach significantly reduces model variance and mitigates the correlation among individual trees.

3.5 Validation

The importance of each variable in the model was determined using the permutation importance method as shown in Eq. (4). This method determines the importance of each parameter based on the model's ability to predict the output in terms of the increase in the error metric by measuring the increase in prediction error [56]. Mathematically, the importance of a feature is computed as:

$$importance_j = MSE_{shuffled} - MSE_{baseline} \tag{4}$$

where:

$importance_j$ is the importance of score of feature *j*.

$MSE_{baseline}$ is the mean squared error of the baseline model.

$MSE_{shuffled}$ is the mean squared error after value of feature *j* are randomly shuffled.

3.6 Accuracy assessment

The accuracy of the model was evaluated using the Receiver Operating Characteristic (ROC) curve, which is a graphical representation that illustrates the model's ability to distinguish between actual events and non-events [57]. The curve is plotted between the true positive rate (TPR), and the false positive rate (FPR). The TPR, also known as sensitivity, is calculated as-

$$TPR = \frac{\mathrm{TP}}{TP + FN} \tag{5}$$

$$FPR = \frac{\mathrm{FP}}{FP + TN} \tag{6}$$

In these formulas, *TP* represents True Positives, *FN* represents False Negatives, *FP* represents False Positives, and *TN* represents True Negatives [58]. The Area Under the Curve (AUC) is a single-number summary of the overall performance of the ROC curve ranging from 0 to 1, where 1 denotes a perfect classifier and a value of 0.5 denotes a non-informative classifier.

Published data (see Table 1) were used for validation. This involved several tests between model outputs and validation data, including Root Mean Square Error (RMSE), Bias, and Index of Agreement (see detail in Supplementary S2).

The RMSE measures provide the standard deviation of the residuals, indicating the magnitude of prediction error.

$$RMSE = \sqrt{\frac{1}{n}\sum\nolimits_{i=1}^{n}(p_i - o_i)^2} \tag{7}$$

The bias measures the average error between predicted and observed values, indicating the systematic deviation of the results. It helps to identify whether predictions are systematically over-or under-estimated.

$$\mathrm{Bias\ b} = \frac{1}{n}\sum\nolimits_{i=1}^{n}(p_i - o_i) \tag{8}$$

The index of agreement (D) quantifies the similarities between two sets of datasets, indicating reliability.

$$D = 1 - \frac{\sum_i^n (p_i - o_i)^2}{\sum_i^n (|\,p_i - o\,|) + (|\,o_i - o|)^2} \tag{9}$$

Here n is the total number of observations, p_i represents model predictions, o_i represents validation observations and o is the mean of the observed data.

3.7 Exposure assessment (building and population)

The validated flood and landslide susceptibility surfaces were independently overlaid with building footprint and population data to quantify direct exposure to single hazards. It provides baseline exposure estimates for medium to very high susceptibility zones prior to multi-hazard integration.

3.8 K-means clustering

To move beyond single hazard assessment, the validated flood and landslide susceptibility data were used as two input parameters for unsupervised k-means clustering. Each spatial unit was represented by its flood probability and landslide probability values. This data-driven approach partitions the national landscape into distinct clusters (k = 3) by minimizing the within-cluster sum of squares:

$$J = \sum_{k=1}^{k} \sum_{x_i \in C_k} \|x_i - \mu_k\|^2 \tag{10}$$

This equation sums up the squared Euclidean distance between each spatial unit and its assigned cluster centroid, optimally grouping areas with similar hazard susceptibility [59]. The number of clusters was set to $k = 3$ to partition the combined flood and landslide susceptibility patterns into three spatially interpretable hazard classes: low-hazard, flood zone and landslide zone. The k-means landslide zone was divided into interaction zones and landslide only zones using Eq. (11) to identify landslide-cluster polygons that share a boundary with flood-cluster polygons. The remaining landslide polygons that do not touch the flood zone constitute the landslide-only zone, yielding four final hazard zones classes that are low-hazard, flood zone, landslide only and interaction zones.

3.9 Multi-hazard spatial adjacency analysis

In Nepal's mountainous geomorphology, the boundary between the landslide-susceptible slope and flood-susceptible river corridors is not an arbitrary geometric artifact but a physically meaningful interaction zone. Landslides occur mostly on steep, fragile hillslopes, while floods are prominent in valleys and lowlands. Each shared boundary corresponds precisely to the slope and floodplain interface where debris from hillslopes enters the fluvial system. The interaction zone is the most plausible location for material transfer, triggering higher risks, as landslide debris enters the river or drainage network at the slope toe that potentially leads to unpredicted compounding effects. Because this study uses the K-means clustering, it produces mutually exclusively interaction zones but, does not include overlapping areas. The shared boundary of flood and landslide zones are therefore used as a proxy to identify geomorphic locus where slope failure and flood hazards are physically coupled.

The spatial adjacency operator selects entire contiguous landslide-cluster polygons that share boundaries with the flood cluster, and the interaction zone propagating through these connected polygons until a spatial break interrupts the chain. The remaining landslide polygons that do not touch the flood cluster are known as the landslide-only zone. Thus, the spatial adjacency operator was applied to delineate multi-hazard interaction zones and critical multi-hazard flow zones.

First, we defined a general spatial adjacent operator as:

$$Adj(B, A) = \{b \in B \,|\, b \cap A = \varnothing \vee \partial b \cap \partial A \neq \varnothing\} \tag{11}$$

where ∂ denotes the topological boundary and $\vee$ denotes the logical disjunction (*OR)*.

Interaction zone is identified by applying this where B represents landslide zone and A represents flood zone. This zone comprises landslide polygons that touches with flood zone.

We again used Eq. (11) to delineate multi-hazard flow zones, mapping upstream to downstream spatial linked corridors. The adjacency operator was applied a second time with A as the flood zone and B as the interaction zone, which identified multi-hazard flow zone, flood prone polygons, spatially linked to an upstream interaction zone. The multi-hazard flow zone comprises downstream flood-susceptible polygons that share boundaries with upstream interaction zones. It referred to as a multi-hazard flow zone because the corridor physically forms both landslide and flood-linked spatial adjacency along the natural drainage pathways. It also reflects that slope failure within the interaction zone may itself be triggered by multiple independent or compounding drivers such as intense monsoon rainfall, seismic ground motion, post-forest fire monsoon induced mudslides, permafrost-thaw degradation or anthropogenic slope cutting, any of which can initiate debris transfer into downstream flood corridor.

3.10 Multi-hazard flow zone and exposure analysis (landcover)

Finally, the multi-hazard flow zones were overlaid with land cover data to quantify impacts on built-up areas and croplands. This stage assesses the integrated exposure of land cover types to compounding hazards, distinct from building and population exposure assessed in single hazard assessment.

4 Results

The flood risk susceptibility model was assessed using an RF model incorporating eleven key conditioning factors. The parameters were ranked by importance as: accessibility > flow accumulation > landform > landcover > slope > hydrological conductivity > flow direction > terrain roughness index > elevation > terrain wetness index > HAND (see Supplementary S9a). The overall accuracy of the flood susceptibility model with the validation dataset was 0.84 as shown in ROC curve (see Supplementary S8a). The susceptibility data were further validated against a hydrological model dataset which was developed by Modelling Exposure Through Earth Observation Routines (METROR's) 100- year return period flood data which has an index of agreement of 74% with an RMSE value 0.48 and a positive bias of 0.18 (see Supplementary S10a). The positive bias indicates that susceptibility model shows stronger agreement with observed data than the METROR dataset exhibits. This might be because the flooded and non-flooded training datasets have captured the recent incidents, whereas the METROR dataset only used DEM, rainfall and landcover as primary input parameters.

Approximately 19% of Nepal's area falls into medium to very high susceptible zones, with major flood inundation in the southern lowland regions, (see Fig. 3a). Flood exposure analysis, on the other hand, revealed significant vulnerability; approximately 900 thousand people and approximately 3.4 million buildings are in the medium to very high-risk zones (see Supplementary Table ST1).

Furthermore, landslide susceptibility was assessed using the RF model incorporating twelve key conditioning factors. These variables are ordered by importance for prediction as: slope > aspect > NDVI > DEM > sand > silt > distance from roads and rivers > TWI > landform > precipitation > land cover and are recognized indicators of slope stability (see Supplementary S9b). The model achieved robust performance with the overall accuracy value of 0.85 as shown in the ROC curve (see Supplementary S8b). The susceptibility model demonstrated strong performance against manually digitized 2015

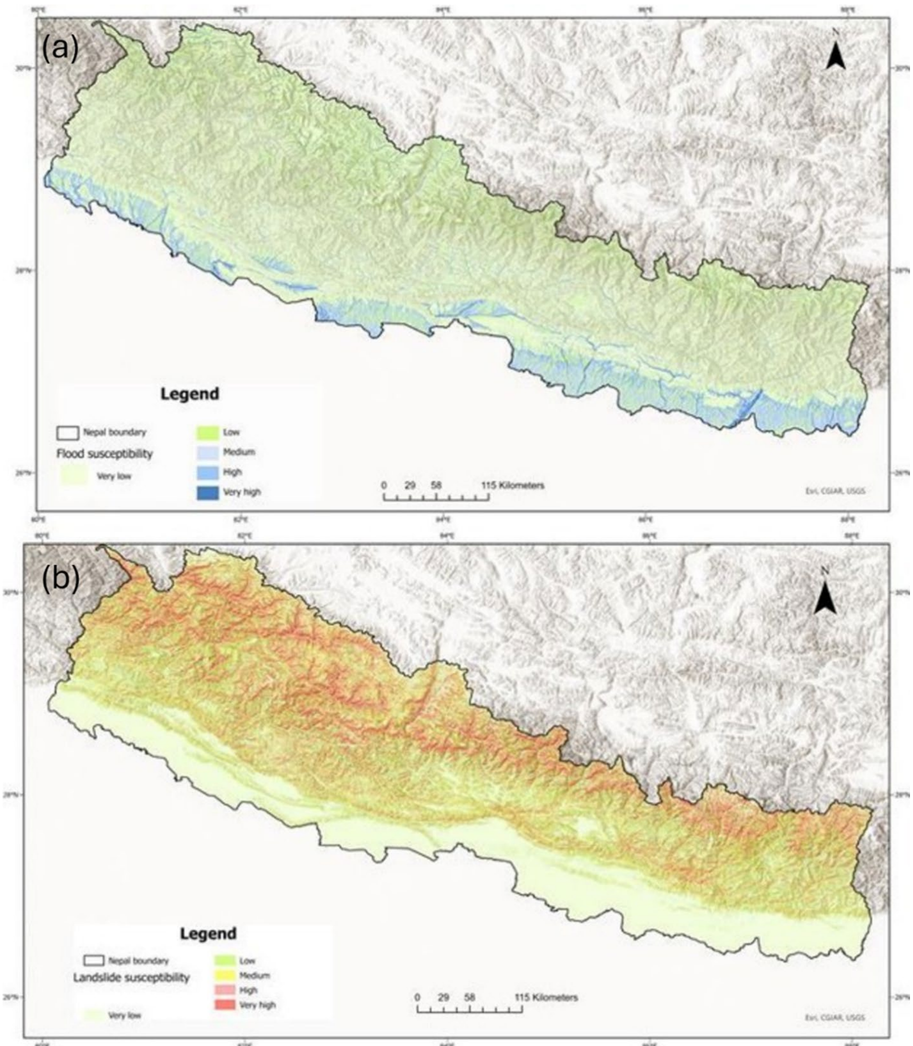

Fig. 3 (**a**) Flood susceptibility map showing zones from very low to very high susceptibility; (**b**) landslide susceptibility map showing zones from very low to very high susceptibility. (Source of Administrative boundary: Department of Survey, Nepal)

earthquake-induced landslide inventory with 81% agreement index, and a small negative bias (−0.18) and RMSE value 0.43 (see Supplementary S10b). The negative bias may be attributed to the inclusion of NDVI as a predictor, which reflects vegetation cover. Nevertheless, the overall agreement with observed landslide and robust discrimination ability indicated that the model provides reliable and conservative estimates for landslide risk susceptibility.

Approximately 40% of the country's area lies within medium to very high-risk zones of landslides, in the northern part (see Fig. 3b). Exposure analysis indicated that approximately 200,000 individuals and 600,000 buildings fall within medium to very high landslide susceptibility zones, revealing localized but critical vulnerabilities, particularly in mountainous and hilly regions of Nepal (see Supplementary Table ST2).

By integrating flood and landslide susceptibility data, this study identified distinct hazard clusters that highlight varying risk profiles across Nepal's diverse topography. In the steep, high-altitude terrain of the northern region (see Fig. 4d), and the middle hills (see Fig. 4a and b), the landscape is dominated by high-density landslide clusters and narrow

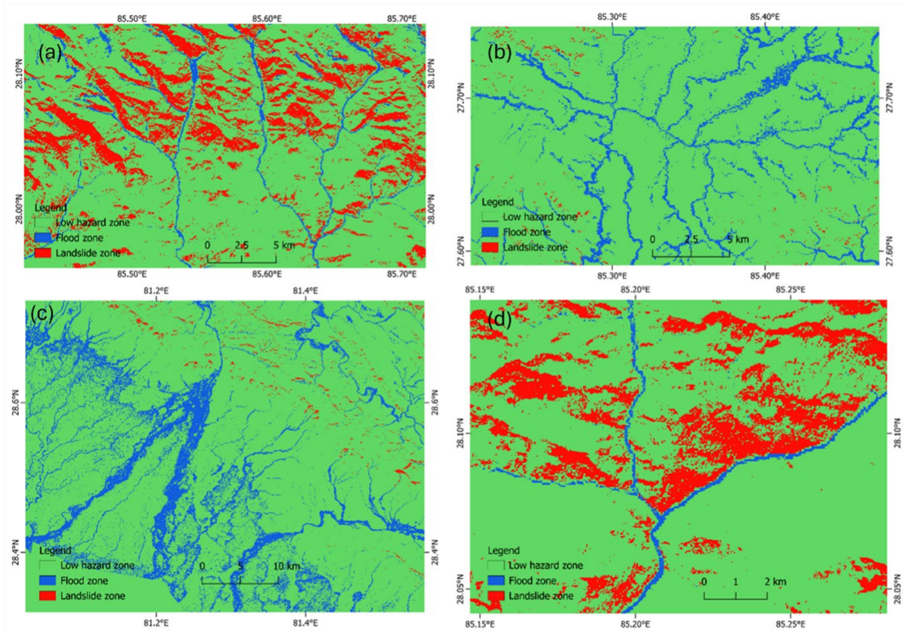

Fig. 4 K-means clustering results showing the spatial distribution of hazard zones across diverse terrain in Nepal: (**a**) concentrated landslide and flood interactions in the Melamchi River area; (**b**) urban flood and hillside landslide zones in the Kathmandu Valley; (**c**) extensive flood zones in the southern Terai Plains (Karnali River basin) in Bardia District; (**d**) high-altitude landslide and river line flood zones in the Humla region

flood corridors. As the topography transitions to the southern part of Nepal (see Fig. 4c), the hazard profile shifts predominantly towards extensive flood-risk zones. Nationally, k-means clustering classify 81% of the total national area as low-hazard zone, 9% is flood zone, and 10% is landslide zone. The k-means clustered landslide zone was subsequently subdivided through spatial adjacency analysis. The analysis identified interaction zone which occupies 5% of total national area and landslide-only zone which do not share a boundary with flood zone accounting the remaining 5% of the total national area(see Fig. 5).

The final stage combined the interaction zone with connected flood prone areas to delineate the multi-hazard flow zones, in which landslide zones are spatially linked to downstream flood zones. The multi-hazard flow zones represent spatial susceptibility-based adjacency rather than physically simulated cascading processes. The multi-hazard flow zone analysis identified approximately 7,588 km^2 of connected multi-hazards zones impacting approximately 88 km^2 of built-up areas (12% of the total bult-up area) and approximately 1,722 km^2 of cropland, underscoring the exposure to human settlements and agricultural lands. The spatial patterns showed minimal risk in the central region from the interaction of both hazards (see Fig. 6e), where stable geomorphic conditions and gentle slopes limit such multi-hazard occurrences. In contrast, steep terrain with dense river networks (see Fig. 6b, c, d, f) exhibits higher likelihood of multi-hazard events.

5 Discussion

This study provides a national-scale assessment of flood and landslide hazard susceptibility and their spatial interaction to identify critical multi-hazard flow zones relevant to human settlement planning and risk informed decision-making in Nepal. By integrating

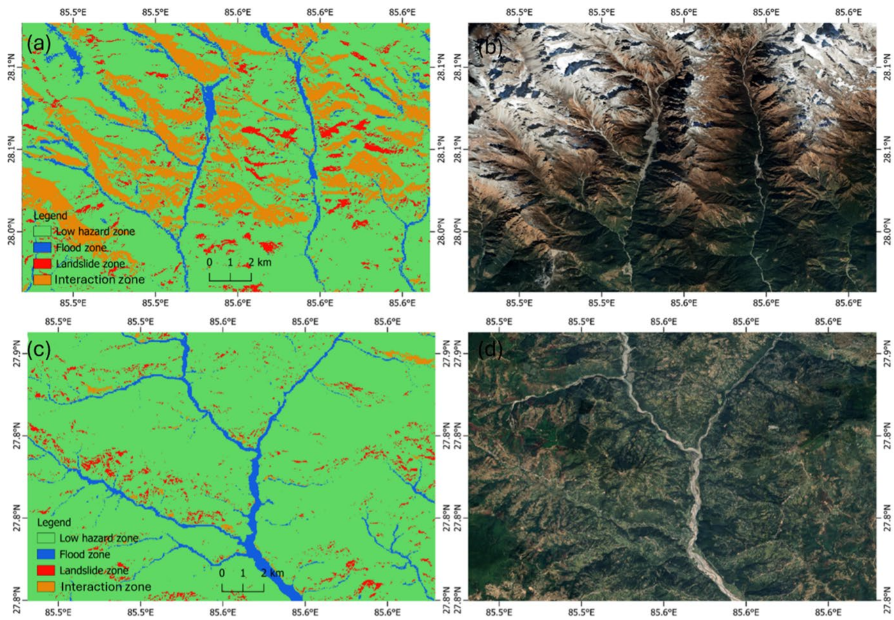

Fig. 5 Showing multi-hazard susceptibility zones derived through spatial adjacency analysis of the k-means clustering results, with corresponding satellite imagery. (**a**) Upper Melamchi area showing interaction zone, flood zone and landslide only zone (**b**) corresponding satellite imagery of the same area; (**c**) lower elevation area of Melamchi, showing flood zones, landslide only zone and interaction zone (**d**) corresponding satellite imagery of same area

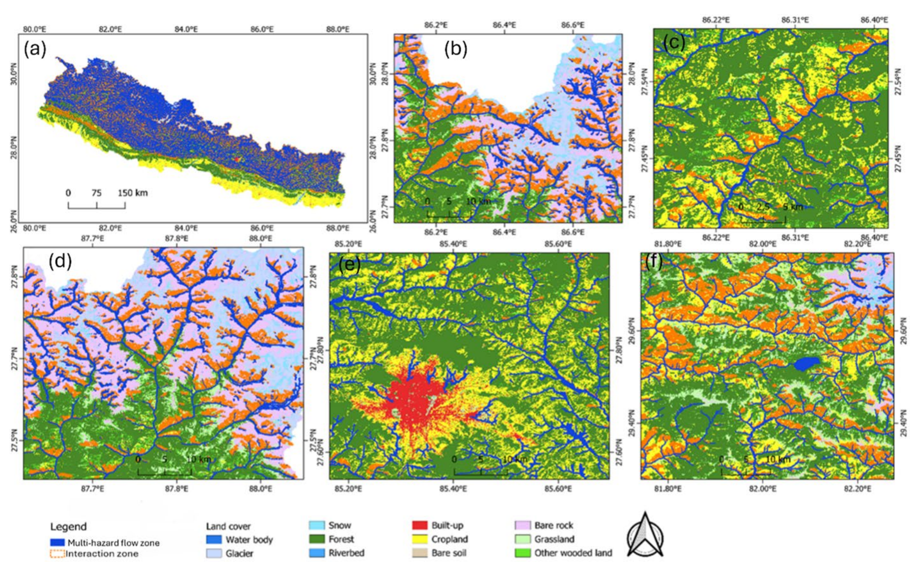

Fig. 6 (**a**) National-scale flood and landslide interaction zone and multi-hazard flow zone across Nepal, (**b**) and (**d**) Detailed regional views of high Himalaya interaction in the Solu-Khumbu (Everest) and Rolwaling regions, (**c**) Hazard interaction in the lower Everest foothills and Okhaldunga areas, (**e**) interaction in Kathmandu Valley area, (**f**) interaction in the high altitude western mountainous region in Mugu district. (Source of Administrative boundary: Department of Survey, Nepal)

diverse geospatial, topographic, climatic, soil, hydrological, anthropogenic and vegetation dataset along with historical hazard inventories, and using RF and k-means clustering, it provides a screening tool to delineate multi-hazard flow zones. The analytical framework complements established methods of expert-driven weighting schemes- such as multi-criteria decision analysis [60] towards a data-driven reproducible approach. Importantly, this shift does not invalidate MCA or Analytical Hierarchy Process (AHP), which retain essential value for local-scale participatory spatial planning, rather than RF probability models extending these foundations to national-scale screening where consistency and reproducibility across heterogenous terrain are paramount.

By using RF probability modeling within the GEE environment, the framework minimizes subjective bias while accommodating multiple conditioning factors simultaneously [34]. The RF model-based results demonstrated high predictive accuracy, benefiting from the hyperparameter tuning and large-scale computation within the GEE. The machine learning approach allowed the incorporation of 11 condition factors for floods and 12 for landslides. The capacity to integrate diverse geospatial, climatic and anthropogenic predictors simultaneously marks a decisive advance over single parameter or expert-weight approaches, increasing both the robustness and generalization of hazard predictions, a trend corroborated by other geospatial applications, such as wetland mapping and temperature estimation [61].

A significant technical advantage of the RF model is its inherent robustness to multicollinearity through bootstrap sampling and random feature selection at each decision node, ensuring that collinearity features do not disproportionately influence the forest consistency [62]. This randomization reduces correlation between the individual trees and decreases overall model variance, allowing effective capture of complex, non-linear relationships between input variables and target hazard without the necessity of separate formal multi-collinearity tests [29]. Consequently, the framework resolves a persistent methodological bottleneck for the Himalayan hazard assessment with ability to process high-dimensional, multi-sources covariates at national extent using cloud-based platforms. The resulting susceptibility maps reveal distinct spatial patterns of flood and landslide risks in Nepal's diverse physiographic regions. In southern Terai and major river valleys, high flow accumulation acts as a primary catalyst for flood risk by concentrating monsoon-driven runoff [63]. On the other hand, areas characterized by high hydrological conductivity, where healthy soil-vegetation complexes facilitate infiltration exhibit significantly lower flood susceptibility. This inverse relationship underscores the protective role of natural land cover in mitigating downstream inundation [64]. In the hilly northern and mountainous regions, susceptibility is dominated by geomorphological triggers like- steep terrain, fragile lithology, and active weathering processes rendering these slopes highly prone to failure [65].

A critical finding of this study is a need for dynamic validation for disaster risk management models within the rapidly evolving Himalayan landscape. Comparing flood susceptibility data with hydrological model, flood inundation maps and landslide susceptibility with an earthquake induced landslide inventory revealed that the positive flood bias indicates a high sensitivity to contemporary hydrological shifts and recent inundation events may be underrepresented in older historical precipitation data which was the primary input of the hydrological modeling. Conversely, the small negative landslide bias is primarily attributed to the stabilizing influence of vegetation regrowth. Since the 2015 Gorkha earthquake, many previously active landslide zones have experienced significant natural recovery [66], which the model has captured via NDVI. The divergent bias pattern however carries consequential implication for disaster management, they demonstrate that flood and landslide systems in Nepal are evolving on different

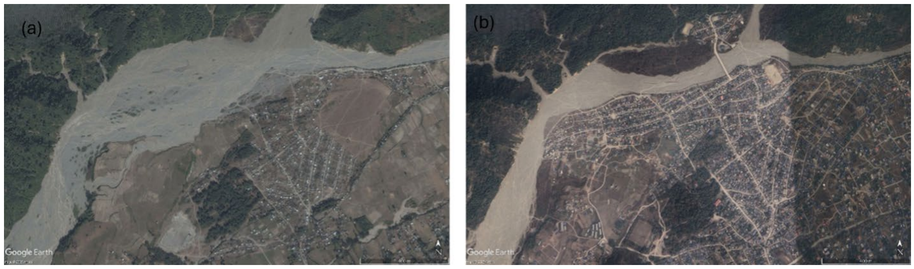

Fig. 7 Urban expansion into the flood-prone terrain along Sardu Khola, Sunsari District, Nepal. (**a**)) Google Earth imagery from 2004 showing sparse settlement and intact agricultural land adjacent to the active river channel. (**b**) Google Earth imagery from 2025 showing expansion of settlements and road networks

post-disturbance trajectories, and the static inventories rapidly lose predictive currency in a region undergoing simultaneous climate impact intensification and ecological recovery. These inherent statistical discrepancies thus highlight that disaster risk management frameworks must transition toward a continuous update cycle that integrates high-resolution inventory.

Flood risk zones would require stricter zoning and proactive adaptation and mitigation strategies such as using nature-based solutions or constructing structural barriers [67, 68], enforcing flood-resilient building codes such as the Federal Emergency Management Agency's principles on building resilient infrastructure and communities [69] or even relocation of high-risk human settlements to safer places. Nepal is yet to include hazard or risk-based zonation in the land use and settlement planning. Current national building regulations rely on river-buffer setbacks (30 m from rivers, 50 m from lakes, 10 m from canals) that are uniform across all terrain types and bear no relationship to topographic susceptibility.

Likewise, for landslide risk zones, specific adaptation and mitigation measures such as controlled land use planning, slope stabilization with bioengineering, restricted construction, restricting hill cutting, reforestation, and plantation could be viable solutions. Further, sustainable land management practices such as terracing, contour farming, wetland restoration, and controlled levees would also mitigate landslides [70–73].

Additionally, increased anthropogenic activities have measurably intensified susceptibility across diverse terrains. Unregulated road construction, land-use conversion, slope cutting, riverbank encroachment, and inadequate drainage infrastructure have collectively diminished geological stability [27, 74–76]. The expansion of human settlements and agriculture intensification near the floodplains in the southern part of Nepal have been constantly increasing exposure to climate extremes, while road networks proliferation in hilly region has destabilized slopes and altered hydrological pathways [77]. Such unplanned and haphazard urbanizations are increasingly triggering local hazards posing high risks to people, infrastructure and ecosystem services [78, 79].

Settlement expansion largely in emerging towns and cities is driven by several factors including rural urban migration, economic opportunities, access to basic services and livelihoods options despite continuing resource constraints, land scarcity and underlying hazard risks in highly susceptible zones. A moderate natural hazard in highly susceptible zones could therefore accelerate and amplify the consequences leading to increased loss and damage. This trajectory is clearly visible along the Sardu Khola region in Sunsari District, where flood plain and riverbed areas once used for agriculture (see Fig. 7a) is now rapidly converting into human settlements with road networks and other infrastructures (see Fig. 7b). Unless policy makers and planners use risk informed susceptibility zonation into municipal land-use plans and the building permits prioritize the development to occur in low-hazard interfluves and elevated terraces for safety and security, the risk will continue to accelerate.

Nepal's federal restructuring has devolved authority to local governments for disaster management and land-use planning, but there exist practical obstacles in implementation. Majority of the municipalities often lack technical capacity to use geospatial tools and products [80], in this case provincial and federal agencies may support in downscaling the information to create user-friendly, accessible, non-technical result-based products such as ward-level atlas that can be easily interpreted and used by local elected officials. Additionally, it cannot be neglected that policy implementations are overshadowed by powerful economic interests most of the time, pushing large scale and critical infrastructure development into hazard prone areas [81, 82]. A strict implementation and monitoring of land-use plans could therefore restrict land conversion and guide unrestricted expansion or encroachment into high susceptible zones. As Nepal's private land tenure secures exclusive right of land use to the owners [83], the government should come up with innovative incentive models like land development (pooling fragmented land parcels to develop improved infrastructure and returning to landowners), land banking (government acquiring and reserving high risk land to mitigating risk) and compensated land redistribution (fair exchange or compensation when people only have land parcels in highly susceptible area) to derisk and ensure safe shelters. These approaches would help to shift the planning from reactive post-disaster relocation to proactive risk screening and risk informed land management.

Past susceptibility studies have focused on single-risk zonation, for instance areas classified as safe zones from flood [84]. However, this paper presents a model for multi-hazard flow zones arising from the interaction of landslides and flood hazards. By autonomously identifying natural groupings within the multi-dimensional data space, the model uses unsupervised k-means clustering algorithms translating susceptibility patterns into actionable architecture distinct to susceptibility zonation without the manual threshold calibration that typically require expert-driven models. Thus, to avoid expert-defined threshold that may overestimate hazard risk in most familiar regions while underestimating in unfamiliar areas, the study used k-means clustering for definitive zonation framework inherently tied to terrain-specific experience [85]. Given that the country has heterogeneous physiographic zones ranging from lowland Terai in the south to high Himalayan slopes in the north, no single expert-defined threshold may capture the terrain diversity without systematic bias. Thus, clustering with $k=3$ value categorizes the landscape into low-hazard, flood and landslide susceptible zones. The interaction zones are subsequently derived through spatial adjacency analysis between flood zones and landslide zones, resulting in four hazard zonation classes. Such data-driven visualization forms a basis for initial screening and evidence-based decision-making for land-use planning, infrastructure investments, and adaptation to risks and hazards. For example, spatial demarcation of low-hazard zones offers comparatively lower risk for development investment or any strategic settlement expansion and critical infrastructure development. Such zones may be distributed across the physiographic regions, districts, and even within high-risk basins. For instance- in the Melamchi river corridor, where interaction and multi-hazard flow zones are concentrated (see Fig. 5), it showed discrete low-hazard pockets on stable interfluves and elevated terraces that are geographically stable. This pattern reinforces that risk-informed development and or settlement planning should be governed by terrain and risk proximity criteria rather than district-level risk generalization. Specifically, areas with flat terrain that is elevated from active flow channels should be prioritized for built-up area expansion, as these interfluve areas demonstrate low flood and landslide susceptibility.

Conversely, multi-hazard interaction zones are highly susceptible areas and require restrictive controls. Development in these areas should be strictly regulated or even declared 'No Go' zones or no service zones. To ensure the restrictions are effective and simultaneously discourage settlement development in high-risk areas, the government ought to enforce regulations for any unauthorized construction within these zones. The identified national-scale susceptibility-based zones should thus be considered as initial screening layers rather than a standalone regulatory boundary. Once a potential or proposed site is screened or high-susceptibility areas are identified, detailed field investigations, including geological verification, geomorphological assessment, local hydrological analysis and consultation with affected communities should be undertaken to understand site-specific fragilities and refine local-level decisions. Such validation is particularly important in heterogenous Himalayan environments where local terrain conditions, climate variables and anthropogenic activities modify the actual hazard conditions. The multi-hazard flow zones represent spatial susceptibility-based adjacency mapping rather than overlapping or physical cascading processes. Therefore, the boundary-adjacency definition serves as a conservative geometry driven connectivity proxy, instead of overlapping deposits indicating stronger sediment delivery potential in fully resolved process-based models. This means that k-means clustering structurally precludes the overlaps, making shared boundaries a pragmatic screening criterion to identify spatially connected locations. Susceptibility derived from such connectivity offers a feasible screening layer to be further field validated and prioritized for localized resource-intensive investigation.

In Nepal's high mountainous regions, the multi-hazard flow zones may hold high potential for cryosphere risk screening. These landscapes are increasingly subject to glacial lake outburst floods and permafrost-thaw-induced slope instability, both of which are influenced by rising temperatures [86, 87]. While the underlying RF model does not explicitly simulate ice dynamics, it captures geomorphological proxies that tend to covary with cryosphere-influenced terrain. This suggests that multi-hazard flow zones could help identify prospective glacier lake flow zones, while interaction zones may highlight regions where permafrost-thaw-induced instability warrants larger attention. This aligns well with the proactive risk management approach of the Sendai Framework highlighting the value of spatial prioritization for monitoring and preparedness in complex systems, even where specific trigger mechanisms are not fully resolved [88, 89]. For example- the Melamchi flood disaster in 2021, revealed cascading hazards driven by anthropogenic and climatic factors which caused several losses to lives and devastated the downstream settlements, markets, transport networks and the newly constructed Melamchi drinking water supply project catering to the urban population in Kathmandu Valley [90]. Similarly, a transboundary flood event in Nepal and China border during July 2025, observed a supraglacial lake outburst from the Purepu Glacier in China's Gyirong County that surged into Rasuwa District in Nepal [91] sweeping away the friendship bridge at Rasuwaghadi, a critical trans-Himalayan economic lifeline connecting trade route between the two countries. Such inferences underscore the current importance of integrating multi-hazard susceptibility zones as spatial proxies to screen and safeguard regional and transboundary corridor development and mitigate future investments to major critical infrastructures too. Hence, delineating multi-hazard flow zones using susceptibility mapping and its regular monitoring could enable preemptive risk screening that may inform governments and local municipalities to plan evacuation and safe shelters [33, 92], develop resilient engineering design and even include financial risk assessment from the planning phase.

On the other hand, the multi-hazard flow zones, where upstream landslide susceptible areas connect spatially with downstream flood exposures provide valuable information to financial institutions and investors to avoid risk related to high investments in infrastructure development, including hydropower projects, transmission corridors, and strategic road networks [93]. The multi-hazard flow zones could eventually be used as preliminary geospatial due diligence screening for spatial risk assessment, pending the validation through site-specific investigations. It can also inform lending decisions and safeguard capital allocations to mega infrastructure projects by identifying places with multi-hazard flow zones that pose higher investment risks. Such screening tools may support evidence based and risk-informed lending to private-sector developers and infrastructure planners enabling pre-loan geological risk assessment and embedding resilient infrastructure designs. However, prevalent context specific data scarcity on multi-hazard risk assessment for critical infrastructure investment and weak penalties for non-compliant developers increases financial risk and uncertainties. For instance, initial screening of critical transport lifelines within multi-hazard zones enables integration of disaster preparedness into supply-chain resilience planning through pre-positioning of emergency supplies and the design of redundant logistics network ultimately contributing to sustainable development goals and the Sendai framework [94]. The evidence-based datasets thus support investors and decision-makers in implementing risk-sensitive planning ensuring that new developments are steered towards safer, low-hazard zones while avoiding high risk interaction and multi-hazard flow zones.

The dataset generated from this study is highly relevant to governments of all tiers for land-use zoning, building code enforcement, emergency response, and resource allocation without specialized geospatial or machine learning knowledge. It largely helps to bridge the gap through pre-defined spatial screening for anticipatory planning and supporting a shift towards anticipatory adaptation and mitigating measures. However, the current operationalization under the federal structure of Nepal faces tangible governance constraints with fragmented information and the real-time connectivity between federal databases and local disaster management committees remain limited. Therefore, the federal agencies should create analytical policy foundations, whereas the provincial units should contextualize implementation outputs, and local planners must execute ground verification in parallel to effective implementation [95].

Despite substantial contribution to risk informed decision making, this study has several limitations that simultaneously define opportunities for future refinement. The multi-hazard flow zones currently represent susceptibility screening derived from spatial adjacency zones rather than overlapping or process-based cascading simulations. So, incorporating landslide-dam formation, breach dynamics, and downstream hydrodynamic propagation within these pre-identified corridors would constitute a valuable refinement to current work. Similarly, while the 400-meter sampling grid was applied to minimize spatial autocorrelation, spatial block cross-validation was not implemented in this study. These gaps provide scope for future work to develop more rigorous geospatial machine learning assessment, while the current indicative metrics provide an initial foundation for national-scale susceptibility screening.

Furthermore, the conditioning parameters were constrained by freely available global and national datasets, some variables such as detailed geological lithology, groundwater table dynamics, and real-time hydrometeorological parameters were not incorporated due to data unavailability. The models were trained on historical datasets that treat hazard patterns as stable over time. Hence, the future work should incorporate shifting climatic conditions to make dynamic maps so that exposure estimates of population, building, and cropland may inherently have less uncertainties. The current uncertainties associated with model prediction variance and classification boundary sensitivity propagate through exposure assessments. Therefore, the reported exposure estimates should be interpreted as indicative screening-level estimates rather than precise measurements of disaster risk or observed hazard impacts. Since this study applies k-means clustering ($k = 3$) together with a GIS-based spatial adjacency approach to delineate multi-hazard interaction zones. Future research could examine different values of k and compare the unsupervised machine learning algorithms to evaluate how alternative clustering strategies influences hazard zonation and interaction mapping. Such investigations would strengthen robustness of the framework and broaden the application of unsupervised machine learning for multi-hazard susceptibility assessment.

Finally, this study quantifies physical exposure but does not address social vulnerability including poverty indices, tenure security layers, and accessibility metrics that would produce more complex risk-informed planning tools. The framework, however, offers a replicable method that can be iteratively improved based on availability of high-resolution dataset and simultaneously addressing the highlighted limitations.

6 Conclusion

The study presents a high-resolution, national-scale assessment for screening flood and landslide hazard susceptibility and their spatial interaction to identify critical multi-hazard flow zones in Nepal by integrating diverse geospatial, topographic, climatic, soil, hydrological, anthropogenic, and vegetation datasets with historical hazard inventories. It combines the RF model with unsupervised k-means clustering and spatial adjacency analysis for hazard screening, particularly suited to data and computing resources constrain mountain environments.

The given framework offers scalable initial screening architecture for multi-hazard susceptibility assessment to prioritize areas for detailed field investigation. The analysis identified distinct spatial patterns where flood risk is predominantly concentrated in the southern Terai, while landslide susceptibility remains highest in the northern hilly and mountainous regions. GIS-based adjacency analysis identified potential interaction zones where landslides are spatially connected to flood zones and critical multi-hazard flow zones linking upstream interaction areas to downstream flood-prone settlements. These results represent susceptibility-based spatial linkages rather than physically simulated cascading hazard process. It also supports subsequent localized hydrodynamic modeling rather than directly resolving the full physical cascading dynamics.

The framework could be used for risk-informed land-use planning, investments to critical infrastructure, and resilient settlement development. It could be also used as geospatial due diligence tool for financial institutions and infrastructure investors, enabling pre-loan geological risk screening, safeguarding hydropower and transport investments, and protecting rural livelihoods. Aligned with the Sendai Framework and Nepal's national disaster risk reduction priorities, the framework bridges national-scale screening with local-level implementation targeting sustainable and resilient development planning. particularly in data-scarce mountain settlements.

Nevertheless, the future iterations should incorporate dynamic data updating, including social vulnerability dimensions, climate non-stationarity, alternative unsupervised clustering approaches, different clustering configurations and process-based hazard modeling. Such enhancements would strengthen the framework to more adaptive and responsive real-time decision support tool.

Supplementary Information

The online version contains supplementary material available at https://doi.org/10.1007/s44288-026-00670-8.

Supplementary Material 1

Acknowledgements

We extend our gratitude to the Editor-in-Chief and the editorial team for the guidance and continued support in the review process. Our heartfelt appreciation goes to the anonymous reviewers who provided constructive feedback and valuable suggestions that greatly improved the methodology and strengthen the arguments in the discussion. Further, we would also like to acknowledge the generous core fund support from the governments of ICIMOD's regional member countries in the Hindu Kush Himalaya- Afghanistan, Bangladesh, Bhutan, China, India, Myanmar, Nepal, and Pakistan and the governments of Austria, Norway, Sweden and Switzerland.

Author contributions

Kabir Uddin, Erica Udas, and Narayan Thapa contributed to the conceptualization and methodology; Kabir Uddin and Erica Udas supervised the study. Narayan Thapa conducted a formal analysis with inputs from Kabir Uddin and Rajesh Bahadur Thapa. Narayan Thapa prepared the original draft of the manuscript. All authors contributed in writing, reviewing, and editing the manuscript.

Funding

This research was supported by ICIMOD's core funds, contributed by the regional member countries in the Hindu Kush Himalaya from the governments of Afghanistan, Bangladesh, Bhutan, China, India, Myanmar, Nepal, and Pakistan, and by the governments of Austria, Norway, Sweden, and Switzerland.

Data availability

The datasets generated and analysed in the current study are available from the corresponding author upon reasonable request.

Declarations

Ethics approval and consent to participate

Not applicable.

Disclaimer

The views and interpretations expressed in this publication are those of the authors and do not necessarily reflect the official views or policies of the International Centre for Integrated Mountain Development (ICIMOD), its regional member countries, or the development partners. The designation of geographical entities and the presentation of material do not imply the expression of any opinion whatsoever on the part of ICIMOD concerning the legal status of any country, territory, city, or area or of its authorities. The administrative boundaries of Nepal used in this study were obtained from the Department of Survey, Government of Nepal, and are presented solely for scientific and cartographic purposes.

AI disclosure statement

During the preparation of this manuscript, the authors used ChatGPT to improve language clarity and readability. All AI-assisted text was carefully reviewed and edited by the authors, who take full responsibility for the final content of the manuscript. The use of AI was limited to language editing and did not contribute to the study design, data collection, data analysis, interpretation of results, or scientific conclusions.

Consent for publication
Not applicable.

Competing interests
The authors declare no competing interests.

Received: 18 December 2025 / Accepted: 30 July 2026
Published online: 04 August 2026

References

1. Wester P, Mishra A, Mukherji A, Shrestha AB. The Hindu Kush Himalaya Assessment. 2019.
2. Alcántara-Ayala I. Cascading hazards and compound disasters. Npj Nat Hazards. 2025. https://doi.org/10.1038/s44304-025-00111-5.
3. Bhochhibhoya S, Maharjan R. Integrated seismic risk assessment in Nepal. Nat Hazards Earth Syst Sci. 2022;22:3211–30. https://doi.org/10.5194/nhess-22-3211-2022.
4. Komolafe AA, Adeyemi AB, Babalola CA, Ebijuoworih EJ, Lawal SO, Odedeyi OB, Akande SO, Adegboyega SA-A. Urbanization driven land cover change and floodplain transformation in the Ogun River Basin using HAND and CA-Markov models. Discover Geoscience 2026. 2026;4(4):1. https://doi.org/10.1007/S44288-026-00529-Y.
5. Khatakho R, Gautam D, Aryal KR, Pandey VP, Rupakhety R, Lamichhane S, Liu YC, Abdouli K, Talchabhadel R, Thapa BR, Adhikari R. Multi-Hazard Risk Assessment of Kathmandu Valley, Nepal, Sustainability 2021, Vol. 13, 13 (2021). https://doi.org/10.3390/SU13105369
6. Gautam D, Thapa S, Pokhrel S, Lamichhane S. Local level multi-hazard zonation of Nepal. Geomat Nat Hazards Risk. 2021;12:405–23. https://doi.org/10.1080/19475705.2021.1879941.
7. Cannon SH, Gartner JE. Wildfire-related debris flow from a hazards perspective. Debris-Flow Hazards Relat Phenom. 2005;363–85. https://doi.org/10.1007/3-540-27129-5_15.
8. Fan X, Scaringi G, Korup O, West AJ, van Westen CJ, Tanyas H, Hovius N, Hales TC, Jibson RW, Allstadt KE, Zhang L, Evans SG, Xu C, Li G, Pei X, Xu Q, Huang R. Earthquake-Induced Chains of Geologic Hazards: Patterns, Mechanisms, and Impacts. Rev Geophys. 2019;57:421–503. https://doi.org/10.1029/2018RG000626.
9. Baral P, Haq MA. Spatial prediction of permafrost occurrence in Sikkim Himalayas using logistic regression, random forests, support vector machines and neural networks. Geomorphology. 2020;371:107331. https://doi.org/10.1016/J.GEOMORPH.2020.107331.
10. Chen C-M, Hollingsworth J, Clark M, Zekkos D, Chamlagain D, Bista S, Siwakoti A, West AJ. The 2021 Melamchi Flood: A massive erosional cascade in the Himalayan Mountains of central Nepal, (2023). https://doi.org/10.21203/rs.3.rs-2766739/v1
11. Maharjan S, Steiner JF, Shrestha AB, Maharjan A, Nepal S, Singh Shrestha M, Bajracharya B, Rasul G, Shrestha M, Jackson M, Gupta N. The Melamchi flood disaster Cascading hazard and the need for multihazard risk management, 2021.
12. Baniya B, Tang Q, Adhikari TR, Zhao G, Haile GG, Sigdel M, He L. Climate change induced Melamchi extreme flood and environment implication in central Himalaya of Nepal. Nat Hazards. 2024;120:11009–29. https://doi.org/10.1007/s11069-024-06645-7.
13. Zuccaro G, De Gregorio D, Leone MF. Theoretical model for cascading effects analyses. Int J Disaster Risk Reduct. 2018;30:199–215. https://doi.org/10.1016/J.IJDRR.2018.04.019.
14. Sutanto SJ, Vitolo C, Di Napoli C, D'Andrea M, Van Lanen HAJ. Heatwaves, droughts, and fires: Exploring compound and cascading dry hazards at the pan-European scale. Environ Int. 2020;134:105276. https://doi.org/10.1016/J.ENVINT.2019.105276.
15. John CK, Pu JH. Urban lifeline resilience under compound hazards: A review on the cascading failures and systemic risk. Lifeline Emerg Saf. 2026;1:9660015. https://doi.org/10.26599/LLES.2025.9660015.
16. Belle JA, Velásquez C, Oxley M, Getiashvili K, Belle JA, Velásquez C, Oxley M, Getiashvili K. Understanding and Integrating Systemic Risk (SR) into Disaster Risk Reduction (DRR) and Risk Informed Development (RID) for Long-Term Resilient Development, (2024). https://doi.org/10.5772/INTECHOPEN.1004915
17. The Government of Nepal Ministry of Home Affairs. Disaster risk reduction national strategic Plan of action, 2018.
18. Vázquez-Tarrío D, Ruiz-Villanueva V, Garrote J, Benito G, Calle M, Lucía A, Díez-Herrero A. Effects of sediment transport on flood hazards: Lessons learned and remaining challenges. Geomorphology. 2024;446:108976. https://doi.org/10.1016/J.GEOMORPH.2023.108976.
19. Rickli C, ETH DF, McArdell B, Badoux A. Phil, Database shallow landslides and hillslope debris flows, (2016).
20. Zhang K, Xue X, Hong Y, Gourley JJ, Lu N, Wan Z, Hong Z, Wooten R. iCRESTRIGRS: A coupled modeling system for cascading flood-landslide disaster forecasting, (2016). https://doi.org/10.5194/hess-2016-143
21. Acharya TD, Mainali SC, Yang IT, Lee DH. Analysis of jure landslide dam, Sindhupalchowk using GIS and Remote Sensing, in: International Archives of the Photogrammetry, Remote Sensing and Spatial Information Sciences - ISPRS Archives, International Society for Photogrammetry and Remote Sensing, 2016: pp. 201–203. https://doi.org/10.5194/isprsarchives-XLI-B6-201-2016
22. Kadel S, Chaudhary S, Khadka SS. Review on assessing climate-change-induced risks to run-of-river hydropower infrastructure in Nepal. Proc IAHS. 2024;387:87–93. https://doi.org/10.5194/PIAHS-387-87-2024.
23. Li D, Lu X, Walling DE, Zhang T, Steiner JF, Wasson RJ, Harrison S, Nepal S, Nie Y, Immerzeel WW, Shugar DH, Koppes M, Lane S, Zeng Z, Sun X, Yegorov A, Bolch T. High Mountain Asia hydropower systems threatened by climate-driven landscape instability. Nat Geoscience 2022. 2022;15:715. https://doi.org/10.1038/s41561-022-00953-y.
24. Thapa P, Thapa N, Thapa M. Deep Learning-Enhanced Flood Risk Mapping for Urban Planning and Disaster Mitigation in the Morang District, Nepal Himalaya, in: 2025: pp. 609–625. https://doi.org/10.1007/978-3-031-95083-4_21
25. United, Nation. Sendai Framework for Disaster Risk Reduction 2015–2030, 2015.
26. Habitat UN. SDG 11: Sustainable cities and Make cities and human settlements inclusive, safe, resilient and sustainable communities, 2023.

27. Dev Acharya T, Yang I, Lee D, Dev T, Tae I, Ha D. GIS-based Landslide Susceptibility Mapping of Bhotang, Nepal using Frequency Ratio and Statistical Index Methods. J Korean Soc Surveying Geodesy Photogrammetry Cartography. 2017;35:357–64. https://doi.org/10.7848/ksgpc.2017.35.5.357.
28. Shrestha BR, Rai RK, Marasini S. Review of Flood Hazards Studies in Nepal. Geographic Base. 2020;7:24–32. https://doi.org/10.3126/tgb.v7i0.34266.
29. Thammaboribal P, Tripathi NK, Lipiloet S. Using of Analytical Hierarchy Process (AHP) in Disaster Management: A Review of Flooding and Landslide Susceptibility Mapping. Int J Geoinformatics. 2025;21:177–96. https://doi.org/10.52939/ijg.v21i4.4091.
30. Le Chan JY, Leow SMH, Bea KT, Cheng WK, Phoong SW, Hong ZW, Chen YL. Mitigating Multicollinearity Problem Its Mach Learn Approach: Rev Math. 2022;10. https://doi.org/10.3390/math10081283.
31. Gnyawali K, Dahal K, Talchabhadel R, Nirandjan S. Framework for rainfall-triggered landslide-prone critical infrastructure zonation. Sci Total Environ. 2023;872:162242. https://doi.org/10.1016/j.scitotenv.2023.162242.
32. Talchabhadel R, Maskey S, Gouli MR, Dahal K, Thapa A, Sharma S, Dixit AM, Kumar S. Multimodal multiscale characterization of cascading hazard on mountain terrain. Taylor Francis. 2023;14:2162443. https://doi.org/10.1080/19475705.2022.2162443.
33. Sharma S, Talchabhadel R, Nepal S, Ghimire GR, Rakhal B, Panthi J, Adhikari BR, Pradhanang SM, Maskey S, Kumar S. Increasing risk of cascading hazards in the central Himalayas. Nat Hazards. 2023;119:1117–26. https://doi.org/10.1007/s11069-022-05462-0.
34. Bera S, Gnyawali K, Dahal K, Melo R, Li-Juan M, Guru B, Ramana GV. Assessment of shelter location-allocation for multi-hazard emergency evacuation. Int J Disaster Risk Reduct. 2023;84:103435. https://doi.org/10.1016/j.ijdrr.2022.103435.
35. Breiman L. Random Forests, 2001.
36. Belgiu M, Drăgu L. Random forest in remote sensing: A review of applications and future directions. ISPRS J Photogrammetry Remote Sens. 2016;114:24–31. https://doi.org/10.1016/J.ISPRSJPRS.2016.01.011.
37. Mosavi A, Ozturk P, Chau KW. Flood prediction using machine learning models: Literature review. Water (Switzerland). 2018;10:1–40. https://doi.org/10.3390/w10111536.
38. Kaya CM, Derin L. Parameters and methods used in flood susceptibility mapping: a review. J Water Clim Change. 2023;14:1935–60. https://doi.org/10.2166/WCC.2023.035.
39. UNDRR. Disaster risk reduction in Nepal: Status report 2019; 1–28. Bangkok, Thailand, United Nations Office for Disaster Risk Reduction, Regional Office for Asia and the Pacific. https://www.preventionweb.net/files/68257_682306nepaldrmstatusreport.pdf
40. Sharma AP, Fu X, Kattel GR. Is there a progressive flood risk management in Nepal? A synthesis based on the perspective of a half-century (1971–2020) flood outlook. Nat Hazards. 2023;118:903–23. https://doi.org/10.1007/S11069-023-06035-5/METRICS.
41. Adhikari BR, Gautam S. A Review of Policies and Institutions for Landslide Risk Management in Nepal. Nepal Public Policy Rev. 2022;2:93–112. https://doi.org/10.3126/nppr.v2i1.48397.
42. Huang Y, Zhao L. Review on landslide susceptibility mapping using support vector machines. Catena (Amst). 2018;165:520–9. https://doi.org/10.1016/J.CATENA.2018.03.003.
43. Franz J, Meyer ICIMOD. (2022). https://rds.icimod.org/Home/DataDetail?metadataId=1973127 (accessed May 17, 2024).
44. Thapa N, Nepali S, Shrestha R, Sanjel S. Time series flood mapping using the Copernicus dataset in Google Earth Engine of the Mountainous Region. Data Brief. 2025;112010. https://doi.org/10.1016/J.DIB.2025.112010.
45. Muñoz-Torrero Manchado A, Allen S, Ballesteros-Cánovas JA, Dhakal A, Dhital MR, Stoffel M. Three decades of landslide activity in western Nepal: new insights into trends and climate drivers. Landslides. 2021;18:2001–15. https://doi.org/10.1007/S10346-021-01632-6/FIGURES/10.
46. ICIMOD. Landslide data of Koshi basin (within Nepal) of 1960 developed through remote sensing approach, ICIMOD (2017). https://doi.org/10.26066/RDS.34424
47. ICIMOD. Landslide data of 14 earthquake affected districts of Nepal [Data set], ICIMOD (2016). https://doi.org/https://doi.org/https://doi.org/10.26066/RDS.31016
48. Theobald DM, Harrison-Atlas D, Monahan WB, Albano CM. Ecologically-Relevant Maps of Landforms and Physiographic Diversity for Climate Adaptation Planning. PLoS ONE. 2015;10:e0143619. https://doi.org/10.1371/JOURNAL.PONE.0143619.
49. Funk C, Peterson P, Landsfeld M, Pedreros D, Verdin J, Shukla S, Husak G, Rowland J, Harrison L, Hoell A, Michaelsen J. The climate hazards infrared precipitation with stations - A new environmental record for monitoring extremes. Sci Data. 2015. https://doi.org/10.1038/sdata.2015.66.
50. NARC, Get digital soil, crop data | NARC, NARC (2020). https://soil.narc.gov.np/getdata (accessed May 21, 2024).
51. Uddin K, Matin MA, Khanal N, Maharjan S, Bajracharya B, Tenneson K, et al. Regional Land Cover Monitoring System for Hindu Kush Himalaya. In: Earth Observation Science and Applications for Risk Reduction and Enhanced Resilience in Hindu Kush Himalaya Region. Springer International Publishing; 2021. p. 103–25. https://doi.org/10.1007/978-3-030-73569-2_6.
52. Boer de Froukje HHS. A High Resolution Soil Map of Hydraulic Properties Version 1.1, 2015. www.futurewater.nl
53. Gaughan AE, Stevens FR, Linard C, Jia P, Tatem AJ. High resolution population distribution maps for Southeast Asia in 2010 and 2015. PLoS One. 2010. https://doi.org/10.1371/journal.pone.0055882.
54. Latpate R, Kshirsagar J, Gupta VK, Chandra G. Adv Sampl Methods. 2021. https://doi.org/10.1007/978-981-16-0622-9.
55. Zarkovich SS, Murthy MN. Sampl Theory Methods. 1969. https://doi.org/10.2307/1402105.
56. Metz CE. Basic principles of ROC analysis, Semin. Nucl Med. 1978;8:283–98. https://doi.org/10.1016/S0001-2998(78)80014-2.
57. Fawcett T. An introduction to ROC analysis, Pattern Recognit. Lett. 2006;27:861–74. https://doi.org/10.1016/J.PATREC.2005.10.010.
58. Greene D, Cunningham P, Mayer R. Unsupervised Learning and Clustering. Cogn Technol. 2008;51–90. https://doi.org/10.1007/978-3-540-75171-7_3.
59. Munier N, Hontoria E. Uses and Limitations of the AHP Method, (2021). https://doi.org/10.1007/978-3-030-60392-2
60. Guo F, Fan L, Zhang C, Xue S. A novel space–spectrum array tile probability random-forest model enhances LULC mapping accuracy on Google Earth Engine: An experiment in Ordos, China. Ecol Inf. 2024;81:102607. https://doi.org/10.1016/J.ECOINF.2024.102607.

61. Hird JN, DeLancey ER, McDermid GJ, Kariyeva J. Google earth engine, open-access satellite data, and machine learning in support of large-area probabilistic wetland mapping. Remote Sens. 2017. https://doi.org/10.3390/rs9121315.
62. Alin A. Robust weighted random forest regression with alternative bootstrap. Stat Outliers Relat Top. 2025;199–220. https://doi.org/10.1201/9781003379881-10/ROBUST-WEIGHTED-RANDOM-FOREST-REGRESSION-ALTERNATIVE-BOOTSTRAP-AYLIN-ALIN.
63. Stromberg JC, Beauchamp VB, Dixon MD, Lite SJ, Paradzick C. Importance of low-flow and high-flow characteristics to restoration of riparian vegetation along rivers in arid south-western United States. Freshw Biol. 2007;52:651–79. https://doi.org/10.1111/J.1365-2427.2006.01713.X.
64. Hobbie SE, Grimm NB. Nature-based approaches to managing climate change impacts in cities. Philos Trans R Soc B Biol Sci. 2020. https://doi.org/10.1098/rstb.2019.0124.
65. Zhang Q, He Y, Zhang L, Lu J, Gao B, Yang W, Chen H, Zhang Y. A landslide susceptibility assessment method considering the similarity of geographic environments based on graph neural network. Gondwana Res. 2024;132:323–42. https://doi.org/10.1016/J.GR.2024.04.013.
66. Pandey HP, Gnyawali K, Dahal K, Pokhrel NP, Maraseni TN. Vegetation loss and recovery analysis from the 2015 Gorkha earthquake (7.8 Mw) triggered landslides. Land Use Policy. 2015. https://doi.org/10.1016/j.landusepol.2022.106185.
67. Khushnood RA, Hamza A, Talha M, Shah A, Khokhar SA, Khan MH, Arsalan Khushnood R, Ahmed T. Advanced structural interventions for slope stabilization and disaster resilience. Discover Geoscience 2025. 2025;3(3):1. https://doi.org/10.1007/S44288-025-00199-2.
68. Howarth M, Smithwick EAH, McPhillips L, Mejia A. Scaling Nature-Based Solutions for Fluvial Floods: A Worldwide Systematic Review. Wiley Interdisciplinary Reviews: Water. 2025;12:e70011. https://doi.org/10.1002/WAT2.70011.
69. Horn DP, Pre-Disaster FEMA, Mitigation. The Building Resilient Infrastructure and Communities (BRIC) Program, Congressional Research Service, Washington, DC, 2022.
70. Hey DL, Philippi NS. Flood reduction through wetland restoration: the Upper Mississippi River Basin as a case history. Restor Ecol. 1995;3:4–17.
71. Keesstra SD, Slovenia SW. Earth Surf Processes Landforms: J Br Geomorphological Res Group. 2007;32:49–65.
72. Nakileza BR, Nedala S. Topographic influence on landslides characteristics and implication for risk management in upper Manafwa catchment, Mt Elgon Uganda. Geoenvironmental Disasters. 2020;7:1–13.
73. Teramura J, Shimatani Y. Advantages of the open levee (Kasumi-tei), a traditional Japanese river technology on the Matsuura river, from an ecosystem-based disaster risk reduction perspective. Water. 2021. https://doi.org/10.3390/w13040480.
74. Bai Y, Sun S, Xu Y, Zhao Y, Pan Y, Xiao Y, Li R. Exploring the dynamic impact of future land use changes on urban flood disasters: A case study in Zhengzhou City. China Geogr Sustain. 2025;6:100287. https://doi.org/10.1016/J.GEOSUS.2025.100287.
75. Dhital YP, Kayastha RB, Shi J. Soil bioengineering application and practices in Nepal. Environ Manage. 2012;51(2):354–64. https://doi.org/10.1007/S00267-012-0003-7.
76. Shrestha M, Sharma S, Shrestha RP. Landslides in the Himalayas: A Comprehensive Review of Hazards, Impacts, and Adaptive Strategies. Rural Reg Dev 2025. 2025;3(Page 10002 3):10002. https://doi.org/10.70322/RRD.2025.10002.
77. Li C, Sun N, Lu Y, Guo B, Wang Y, Sun X, Yao Y. Rev Urban Flood Risk Assess Sustain (Switzerland). 2023;15. https://doi.org/10.3390/SU15010765.
78. Regmi S, Dahal RK. Consequences of slope instability and existing practices of mitigation in hydropower projects of Nepal. Geoenvironmental Disasters 2024. 2024;11(11):1. https://doi.org/10.1186/s40677-024-00289-2.
79. Poudel DP, Blackburn S, Manandhar R, Adhikari B, Ensor J, Shrestha A, Timsina NP. The urban political ecology of 'haphazard urbanisation' and disaster risk creation in the Kathmandu valley, Nepal. Int J Disaster Risk Reduct. 2023;96:103924. https://doi.org/10.1016/J.IJDRR.2023.103924.
80. Lamichhane K, Karki S, Sharma K, Khadka B, Acharya B, Biswakarma K, Adhikari S, Kc R, Danegulu A, Bhattarai S, Regmi A, Subedi M, Bhattarai PK. Unraveling the causes and impacts of increasing flood disasters in the kathmandu valley: Lessons from the unprecedented September 2024 floods. Nat Hazards Res. 2025;5:875–97. https://doi.org/10.1016/J.NHRES.2025.04.001.
81. Thapa RB, Matin MA, Bajracharya B. Capacity building approach and application: utilization of earth observation data and geospatial information technology in the Hindu Kush Himalaya. Front Environ Sci. 2019. https://doi.org/10.3389/fenvs.2019.00165.
82. Shrestha R, Zevenbergen J, Banskota M, Tuladhar A, Netherlands T. Decades of Struggle for Space. About the Legitimacy of Informal Settlements in Urban Areas; 2014.
83. Acharya BR. Exploring the Causes of Squatting in the Balkhu Corridor of Kathmandu. Dhaulagiri J Sociol Anthropol. 2024;16–27. https://doi.org/10.3126/dsaj.v18i01.67516.
84. 2021 Government of Nepal, Land Act, English. 1964. www.lawcommission.gov.npwww.lawcommission.gov.np
85. World Bank Group. Land Use Planning for Urban Flood Risk Management, 2017.
86. Vierkant T. Core Argument and Methodology, The Tinkering Mind (2022) 3–30. https://doi.org/10.1093/OSO/9780192894267.003.0001
87. Baral P, Allen S, Steiner JF, Gurung TR, McDowell G. Climate change impacts and adaptation to permafrost change in High Mountain Asia: a comprehensive review. Environ Res Lett. 2023. https://doi.org/10.1088/1748-9326/acf1b4.
88. Shrestha F, Steiner JF, Shrestha R, Dhungel Y, Joshi SP, Inglis S, Ashraf A, Wali S, Walizada KM, Zhang T. A comprehensive and version-controlled database of glacial lake outburst floods in High Mountain Asia. Earth Syst Sci Data. 2023;15:3941–61. https://doi.org/10.5194/ESSD-15-3941-2023.
89. Mizutori M, Reflections on the Sendai Framework for Disaster Risk Reduction. Five Years Since Its Adoption. Int J Disaster Risk Sci. 2020;11:147–51. https://doi.org/10.1007/s13753-020-00261-2.
90. Duwadi S, Pani Adhikari D, Raj Dhital M, Parajuli N. Assessment of the 2021 debris flow and flood related loss and damage in Melamchi Watershed of Central Nepal, 2024.
91. Zhang Q, Hu K, Liu S, Wei L, Zhang X. Remote sensing interpretation of causes and dynamics of the Gyirong outburst flood disaster, Tibet, on July 8, 2025. Nat Hazards 2026. 2026;122:7122. https://doi.org/10.1007/S11069-026-08081-1.
92. Uddin K, Matin MA. Potential flood hazard zonation and flood shelter suitability mapping for disaster risk mitigation in Bangladesh using geospatial technology. Progress Disaster Sci. 2021;11:100185. https://doi.org/10.1016/j.pdisas.2021.100185.

93. Thapa N, Pant P, Prasai R, Mahata A, Dulal S. Sustainable land use planning in developing countries using GIS and multi-criteria analysis: a case study of Lalitpur district, Nepal, City and Built Environment 2025 3:1 3 (2025) 1–20. https://doi.org/10.1007/S44213-025-00050-X
94. Chauhan V, Gupta L, Dixit J. Machine learning and GIS-based multi-hazard risk modeling for Uttarakhand: Integrating seismic, landslide, and flood susceptibility with socioeconomic vulnerability. Environ Sustain Indic. 2025;26:100664. https://doi.org/10.1016/J.INDIC.2025.100664.
95. Waters D. Supply chain risk management: vulnerability and resilience in logistics, 2011.

Publisher's note